Autonomous Quantum Error Correction of Gottesman-Kitaev-Preskill States

Dany Lachance-Quirion[*], Marc-Antoine Lemonde, Jean Olivier Simoneau, Lucas St-Jean, Pascal Lemieux,
Sara Turcotte, Wyatt Wright, Amélie Lacroix, Joëlle Fréchette-Viens, Ross Shillito, Florian Hopfmueller,
Maxime Tremblay, Nicholas E. Frattini, Julien Camirand Lemyre, and Philippe St-Jean

Nord Quantique, Sherbrooke, Québec J1J 2E2, Canada

The Gottesman-Kitaev-Preskill (GKP) code encodes a logical qubit into a bosonic system with resilience against single-photon loss, the predominant error in most bosonic systems. Here we present experimental results demonstrating quantum error correction of GKP states based on reservoir engineering of a superconducting device. Error correction is made fully autonomous through an unconditional reset of an auxiliary transmon qubit. We show that the lifetime of the logical qubit is increased from quantum error correction, therefore reaching the point at which more errors are corrected than generated.

Improving error correction schemes is a central challenge toward the development of fault-tolerant quantum processors. A high-quality bosonic mode controlled by an auxiliary nonlinear element has proven a valid candidate to replace the standard two-level system approach [1–4], bringing to life the visionary proposal of Gottesman *et al.* for error correction at the individual qubit level [5–11]. This approach is gaining momentum, thanks in part to recent experiments showing an increase in logical lifetime of bosonic codes through error correction [12–18], and promises to ease the requirements on number of modes needed for useful quantum computation [7–9].

Most of the recent bosonic code error correction experiments in superconducting circuits have relied on measurements of the auxiliary nonlinear element to condition real-time feedback and feed-forward operations [12–14,17,18], thereby introducing challenges related to measurement fidelity and complexity and latency of control electronics. Fully autonomous quantum error correction protocols for bosonic codes alleviate those challenges by reducing reliance on measurement of the auxiliary [15,16,19–21].

Recent work introduced more efficient protocols for error correction of finite-energy Gottesman-Kitaev-Preskill (GKP) qubits [16,22]. With this approach, an improvement of the logical lifetime of the GKP qubit by a factor of 2.27 over the logical lifetime of the Fock encoding was demonstrated [17]. There, the reset of the auxiliary qubit, necessary for the reservoir-engineered quantum error correction (QEC) protocol, was implemented with a measurement of the auxiliary followed by feedback and feed-forward operations on both the auxiliary and the bosonic mode.

In this Letter, we present experimental results demonstrating a fully autonomous QEC protocol of a GKP qubit through a feedback-free reset of the auxiliary transmon qubit. Despite the auxiliary having 10 times stronger relaxation rate than the bosonic mode, we demonstrate an increase of the logical lifetime of the GKP qubit when applying error correction. Experimental results are supported with numerical simulations that show quantitative agreement for both the initialization and the quantum error correction of GKP states.

A multielement superconducting device is used to experimentally realize autonomous QEC of GKP states in a circuit quantum electrodynamics architecture [23]. The bosonic mode is hosted inside a three-dimensional seamless coaxial cavity [24] made out of high-purity aluminum [Fig. 1(a)]. The fundamental $\lambda/4$ mode of the cavity, hereafter the "storage mode," has a lifetime of $T_{1s} = 0.34$ ms. A chip in the coaxial line architecture is used to provide the nonlinearity required to control the storage mode [25]. A transmon qubit, a resonator, and a Purcell filter are fabricated on this silicon chip [23,26]. The auxiliary transmon qubit has a relaxation time $T_{1q} = 33$ μs and echo coherence time $T_{2q} = 48$ μs. The resonator, used for readout and reset of the auxiliary transmon [27–29], has a fundamental $\lambda/2$ mode that is overcoupled through the Purcell filter to an output port with total decay rate $\kappa_r/2\pi = 1.7$ MHz. The chip is slightly inserted inside the microwave cavity to overlap with the storage mode, leading to a dispersive shift of $2\chi_{sq}/2\pi = -22$ kHz per excitation [24,25].

The GKP states initialized and error corrected in this Letter are the six finite-energy cardinal states $|\pm\bar{\mu}\rangle$ with $\bar{\mu} \in \{\bar{X}, \bar{Y}, \bar{Z}\}$ of finite-energy parameter Δ. As shown in Fig. 1(b), we experimentally prepare these states by applying a circuit with alternating auxiliary rotations and conditional displacements of the storage mode, exploiting that such circuits enable approximate universal control of the storage mode [30]. Conditional displacements, which
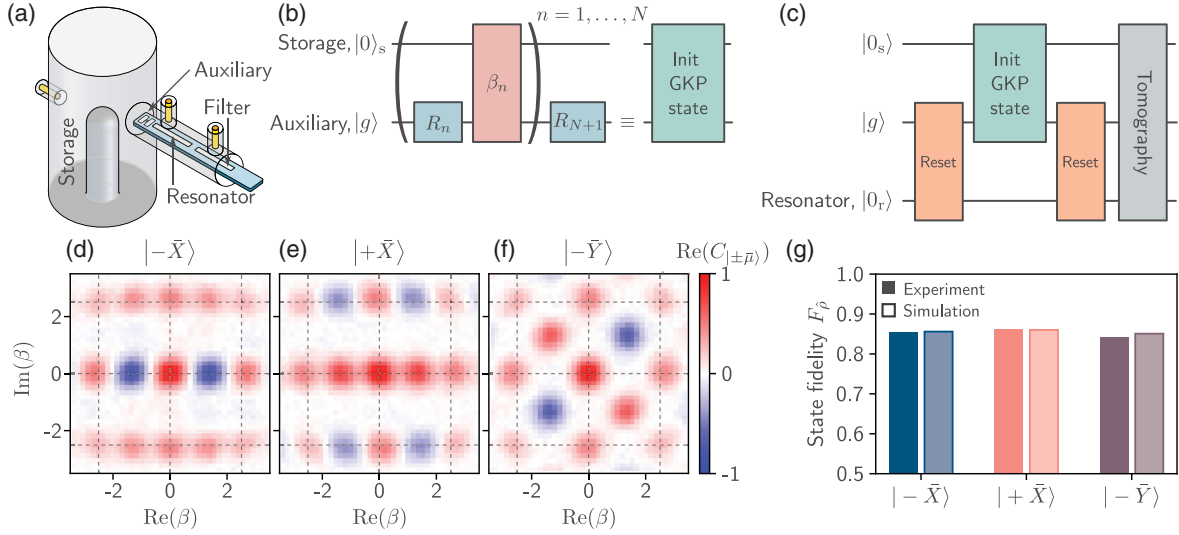
FIG. 1. (a) Schematic of hardware architecture. The storage mode, in which the GKP code is encoded, is the fundamental mode of a coaxial cavity dispersively coupled to an auxiliary transmon qubit. The auxiliary is also dispersively coupled to an on-chip resonator used for readout and reset. (b) Protocol for the initialization of GKP logical states with a depth-N circuit. Each layer n consists of an auxiliary rotation of parameter R_n and a conditional displacement on the storage mode of parameter β_n. (c) Protocol for measurement of the characteristic function of initialized GKP logical states. Real part of the characteristic function $\text{Re}(C_{|\pm\bar{\mu}\rangle})$, of GKP logical states (d) $|-\bar{X}\rangle$, (e) $|+\bar{X}\rangle$, and (f) $|-\bar{Y}\rangle$ for $\Delta = 0.36$ using a circuit with a depth $N = 9$, leading to an initialization duration of 7.86 μs excluding resets. (g) State fidelity estimated from state reconstruction given measured (d)–(f) and simulated characteristic functions.

displace the state of the storage mode with a sign conditioned on the state of the auxiliary, are implemented with the echoed conditional displacement protocol in 0.85 μs [14,30]. The initialization protocol parameters for the auxiliary rotation and conditional displacements of the storage mode are found using optimization for a given target state $|\pm\bar{\mu}_0\rangle$ and parameter Δ [31].

We perform tomography of the prepared states by measuring the characteristic function $C_{|\pm\bar{\mu}\rangle}(\beta)$ of the storage mode using the auxiliary initialized in $|g\rangle$, where β is the amplitude of the tomography conditional displacement [14,30,39]. The complete protocol for initialization and tomography of GKP logical states is shown in Fig. 1(c). The initial reset, whose details are discussed later, decreases to probability of the auxiliary to be in its excited state $|e\rangle$ from the thermal population of 0.4% to 0.1%. The reset after the initialization protocol approximately ensures that the tomography protocol starts with the auxiliary in $|g\rangle$ even if errors have occurred during the initialization protocol.

The real part of the characteristic function for the GKP states $|-\bar{X}\rangle$, $|+\bar{X}\rangle$, and $|-\bar{Y}\rangle$ are shown in Figs. 1(d)–1(f) for finite-energy parameter $\Delta = 0.36$, corresponding to an average number of photons $\bar{n}_s = 3.5$ and squeezing of 8.9 dB. The remaining cardinal states of the GKP qubit are obtained by a rotation in phase space with $\beta_n \rightarrow i\beta_n$. We evaluate the fidelity of initialized GKP logical states with $F_{\hat{\rho}} = \text{Tr}\sqrt{\hat{\rho}^{1/2}\hat{\rho}_{\text{target}}\hat{\rho}^{1/2}}$, where $\hat{\rho}$ is the density matrix obtained via state reconstruction from

measurements of the characteristic function [40], and $\hat{\rho}_{\text{target}}$ is the density matrix of ideal finite-energy GKP logical states [Fig. 1(g)]. State fidelity averaged over the cardinal states reaches 85(1)%. By fitting fidelities from numerical simulations to the experimentally estimated fidelities, we estimate an intrinsic dephasing of the storage mode at a rate $\kappa_{s\phi} = (110 \text{ ms})^{-1}$, which is consistent with the value of Ref. [30]. Storage mode dephasing, amplified during large displacements [30], explains a preparation infidelity of 6.4%, while decay of the auxiliary leads to an additional 4.0% [31].

While the full tomography in phase space is useful to estimate the density matrix and state fidelity from reconstruction, the logical information of the GKP qubit can be measured more efficiently. The logical fidelity F_L may be expressed as

$$F_L = \frac{1}{2} + \frac{1}{12} \sum_{\hat{\mu}_0 \in \{\hat{X}_0, \hat{Y}_0, \hat{Z}_0\}} (\langle\hat{\mu}_0\rangle_+ - \langle\hat{\mu}_0\rangle_-), \quad (1)$$

where $\langle\hat{\mu}_0\rangle_\pm = \langle\pm\bar{\mu}|\hat{\mu}_0|\pm\bar{\mu}\rangle$ is the expectation value of the infinite-energy Pauli operator $\hat{\mu}_0$ when a logical state $|\pm\bar{\mu}\rangle$ with $\bar{\mu} \in \{\bar{X}, \bar{Y}, \bar{Z}\}$ is prepared [17,41]. The Pauli expectation value corresponds to the real part of the characteristic function $C_{|\pm\bar{\mu}\rangle}(\beta_{\hat{\mu}_0})$ of the state $|\pm\bar{\mu}\rangle$ with $\beta_{\hat{X}_0} = \ell/\sqrt{8}$, $\beta_{\hat{Y}_0} = (1 + i)\ell/\sqrt{8}$, and $\beta_{\hat{Z}_0} = i\ell/\sqrt{8}$ with $\ell = 2\sqrt{\pi}$ for the square GKP qubit [22,42]. After state preparation, the logical fidelity reaches 84%.

A reset of the auxiliary qubit is required for error correction of GKP states based on reservoir engineering, as it constitutes the dissipative channel through which entropy is evacuated [22]. The error correction can be made completely autonomous using a microwave-activated unconditional reset [27–29]. As shown in Fig. 2(a), the reset is based on swapping two excitations from the auxiliary to a single readout resonator excitation through an effective $|f0_r\rangle \leftrightarrow |g1_r\rangle$ transition of the coupled system [27,28,43], where $|kn_r\rangle = |k\rangle \otimes |n_r\rangle$ corresponds to the
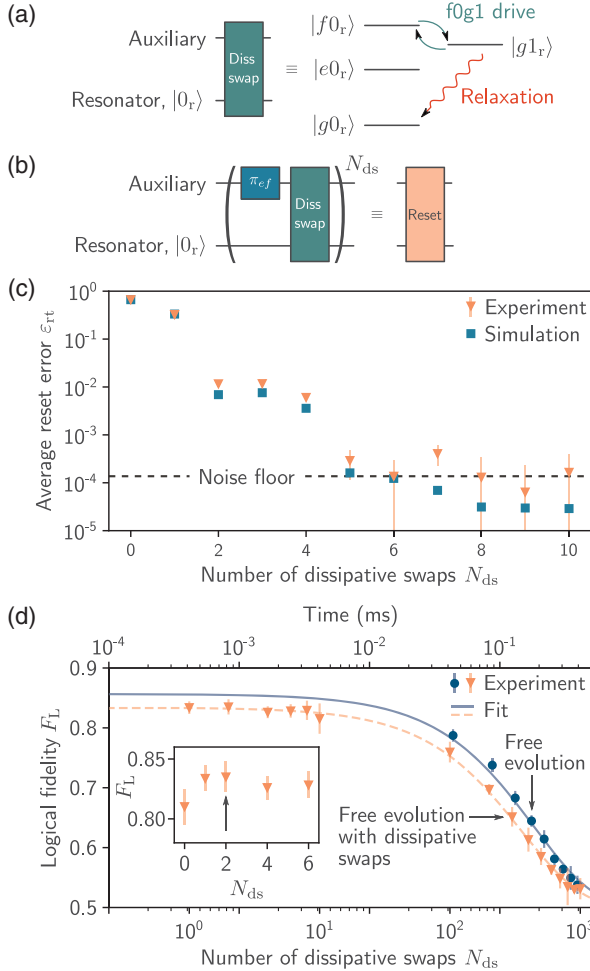

(a)

(b)

(c)

(d)

FIG. 2. (a) Dissipative swap between the auxiliary qubit and the resonator enabled by an effective $|f0\rangle_r \leftrightarrow |g1\rangle_r$ transition, followed by relaxation as $|g1\rangle_r \rightarrow |g0\rangle_r$. (b) Reset protocol with N_{ds} dissipative swaps. (c) Average reset error ε_{rt} as a function of N_{ds} measured experimentally (orange) and obtained from numerical simulations (teal). The horizontal dashed line indicates the experimental noise floor of 4×10^{-4}. (d) Logical fidelity F_L measured as a function of free evolution time (blue, top axis) or number of dissipative swaps (orange, bottom axis). Plain and dashed lines show fits to the data from which logical lifetimes T_L of 0.176 and 0.143 ms are obtained for free evolution without and with dissipative swaps, respectively. The limit $F_L \rightarrow 0.5$ represents a fully decohered logical channel. Inset: enlarged to highlight the optimal value of $N_{ds} = 2$.

qubit state $|k \in \{g, e, f, \ldots\}\rangle$ and resonator Fock state $|n_r \in \{0_r, 1_r, 2_r, \ldots\}\rangle$. The resulting photon in the resonator dissipates to the environment through $|g1_r\rangle \rightarrow |g0_r\rangle$ on a timescale corresponding to resonator lifetime $T_{1r} = 1/\kappa_r = 92$ ns. The complete process is an effective auxiliary-resonator dissipative swap.

To reset the first excited state $|e\rangle$ of the auxiliary, we prepend the dissipative swap with a π pulse addressing the $|e\rangle \leftrightarrow |f\rangle$ transition [Fig. 2(b)]. This base sequence can be repeated to reset the second excited state $|f\rangle$ of the qubit. The reset protocol—which takes 414 ns per swap including resonator decay—is repeated N_{ds} times to decrease the reset error. Ideally, the qubit ends up in the ground state after the reset regardless of the initial state $|k \in \{g, e, f\}\rangle$ for $N_{ds} \geq 2$.

The average reset error, defined as

$$\varepsilon_{rt} = \frac{1}{3} \sum_{k \in \{g,e,f\}} (1 - p_{g|k}), \qquad (2)$$

where $p_{g|k}$ is the probability of the qubit being in the ground state $|g\rangle$ when preparing state $|k\rangle$, is estimated as a function of the number of dissipative swaps N_{ds} with the storage mode in equilibrium. We estimate the probabilities $p_{g|k}$ and the reset error ε_{rt}, shown in Fig. 2(c), with a procedure aiming at factoring out state preparation and measurement errors as described in the Supplemental Material [31].

When the storage mode is not in a Fock state $|n_s\rangle$, undesired entanglement is formed between auxiliary and storage mode during the reset process due to their always-on dispersive interaction. For instance, dispersion of the auxiliary energy levels leads to an increase of the reset error for $N_{ds} = 2$ from 1.4% in the vacuum to 2.8% in the presence of a GKP logical state $|-\bar{X}\rangle$ [31].

The optimal number of dissipative swaps per reset for QEC needs to be chosen to achieve a low reset error, while avoiding any adverse effects on the GKP state. Figure 2(d) shows that we observe a decrease of the logical fidelity when replacing free evolution of GKP states with a reset composed of N_{ds} dissipative swaps [31]. Given that the reset process should generate an identity operation on the storage mode when the auxiliary is in $|g\rangle$, the observed decrease of the logical lifetime hints at an additional dephasing mechanism whose investigation is left to future work. The inset of Fig. 2(d) indicates that $N_{ds} = 2$ maximizes the logical fidelity of the GKP qubit. This value is thus used throughout the Letter.

The quantum error correction protocols for GKP states proposed in Ref. [22] engineer a set of two dissipators whose ground state manifold corresponds to the desired logical manifold even in the presence of single-photon loss in the storage mode. A single round of the small-big-small (sBs) protocol approximates each of the required dissipators by a depth-3 circuit of auxiliary rotations and conditional displacements, followed by a dissipative
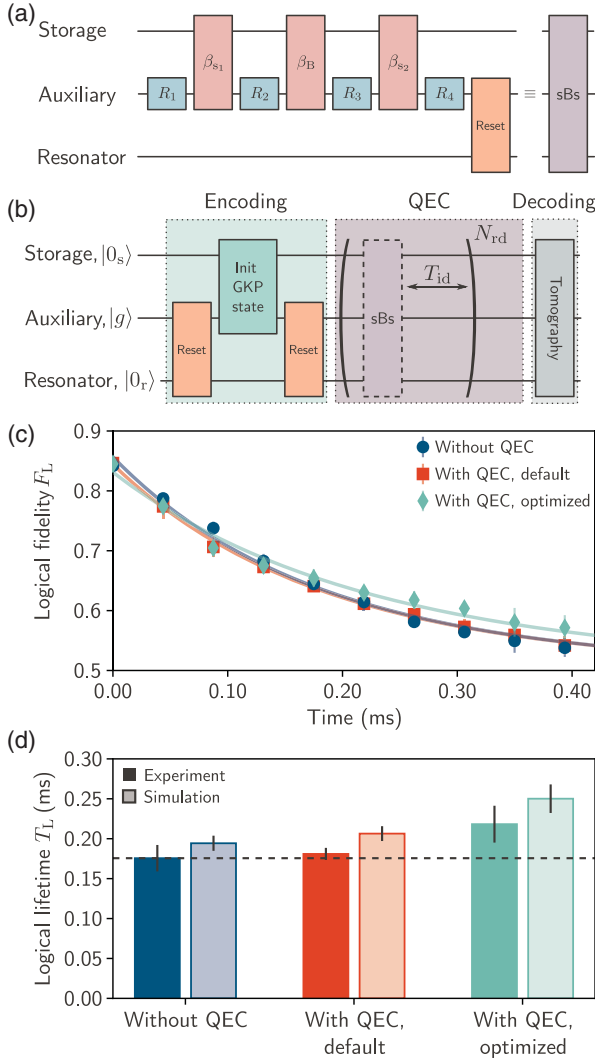
FIG. 3. (a) Quantum error correction protocol based on the sBs protocol composed of auxiliary rotations, conditional displacements, and a reset of the auxiliary. (b) Protocol used to measure the logical lifetime. After initialization of a GKP logical state (encoding), the sBs protocol is either applied (with QEC) or not (without QEC) N_{id} times. An extra idle time T_{id} between each round is added in both cases. The GKP qubit Pauli expectation value $\langle \hat{\mu}_0 \rangle_{\pm}$ is measured for states $|\pm \bar{u}\rangle$ (decoding). (c) Logical fidelity F_L measured as a function of time without QEC (blue) and with default (red) or optimized sBs protocols (turquoise) for $T_{id} = 40$ μs. The full lines show the decay of the logical fidelity obtained from a fitting procedure [31]. The data without QEC are the same as in Fig. 2(d). (d) Logical lifetime T_L obtained experimentally (dark bars) and numerically (pale bars). The horizontal dashed line corresponds to the logical lifetime without QEC.

operation implemented through unconditional reset of the auxiliary [Fig. 3(a)]. The parameters of the sBs protocol are $\boldsymbol{\beta}_{sBs} = (\beta_{s_1}, \beta_B, \beta_{s_2})$ with

$$\beta_{s_{1,2}}^{(n)} = \frac{i^{(n-1)} \ell \sinh \Delta_{sBs}^2}{2\sqrt{2}}, \qquad \beta_B^{(n)} = \frac{i^n \ell \cosh \Delta_{sBs}^2}{\sqrt{2}}, \qquad (3)$$

for round n and $\mathbf{R}_{sBs} = [+(i\pi/2), +(\pi/2), -(\pi/2), -(i\pi/2)]$ [22]. We use the effective finite-energy parameter Δ_{sBs} as an optimization parameter with a default value of Δ. After each round, the conditional displacements are rotated a quarter turn via the i^n factor in order to implement both required dissipators while symmetrizing the conditional displacements signs.

Our main experiment measures the logical lifetime of the quantum memory. The protocol, shown in Fig. 3(b), is composed of an encoding step through the initialization protocol [Fig. 1(c)], followed by N_{rd} rounds of quantum error correction with the sBs protocol [Fig. 3(a)], and finally a decoding step through measurement of the Pauli expectation value of the GKP qubit. We insert an idle time T_{id} after each round of error correction to allow us to balance correctable single-photon loss from the storage mode and uncorrectable errors introduced by auxiliary decay during the sBs protocol [12]. The duration of the QEC step is given by $T = N_{rd} T_{rd}$, with time per round $T_{rd} = T_{sBs} + T_{id}$, with $T_{sBs} = 3.738$ and $T_{id} = 40$ μs. This corresponds to a photon loss probability per round $\kappa_s T_{sBs} = 1.1 \times 10^{-2}$ and $\kappa_s T_{rd} = 1.3 \times 10^{-1}$.

Figure 3(c) shows the logical fidelity measured experimentally without and with QEC, both with default and optimized sBs protocols. We obtain the optimized protocol by maximizing logical fidelity at $N_{rd} = 4$ in a closed-loop optimization. The optimization parameters are the effective finite-energy parameter Δ_{sBs}, the scaling of the second small displacement, parametrized by the ratio $|\beta_{s_2}|/|\beta_{s_1}|$, and a state rotation per round [31]. The optimized ratio $|\beta_{s_2}|/|\beta_{s_1}| = 1.82$ is found to be significantly different from the value of the default protocol, yet consistent with results in Ref. [17].

Figure 3(d) shows the logical lifetime obtained experimentally and from numerical simulations from the decay of the logical fidelity [31]. The gap between experimental and simulation values, when not allowing any fitting parameters, indicates that some effects are not captured in simulation. The logical lifetime is increased by 21% through closed-loop optimization. Most importantly, the logical lifetime is increased by 24% when applying the optimized QEC protocol compared to the lifetime of the same states without QEC, thus demonstrating that our autonomous error correction protocol corrects more errors than it generates. The logical lifetime with optimized QEC, $T_L^{opt} = 0.218(23)$ ms, is nevertheless lower than for the Fock encoding $\{0, 1\}$ with $T_L^{Fock} = 0.482$ ms in simulations [31].

The gain from QEC in our experiment is limited by bit flips of the auxiliary transmon during conditional displacements of the sBs protocol, which can cause logical errors not protected against by the GKP code [14,17,22]. The presence of this error channel forces the insertion of idle times $T_{id} \gg T_{sBs}$ for optimal performance, which in turn limits the rate of error correction and the protection against single-photon loss in the storage mode. Both aspects call

for reducing the rate of auxiliary errors with longer-lived transmons [17,44] or fault-tolerant error syndrome extraction [45] with noise-biased auxiliaries [46–50] and reducing their impact on logical states through more robust encoding of GKP qubits [51].

Irrespective of the error rate of the auxiliary, reducing the probability of single-photon loss during the sBs protocol, $\kappa_s T_{sBs} = 1.1 \times 10^{-2}$ here, would increase the gain from QEC [22]. For a fixed single-photon loss rate κ_s, improving $\kappa_s T_{sBs}$ would require faster conditional displacements, either through optimization of the echoed conditional displacement protocol [30] or through alternative methods to implement conditional displacements in superconducting circuits [48,49,52–56]. Finally, the advantages of the fully autonomous approach presented here and the measure-and-feedback approach of Ref. [17] could be combined. Indeed, by using a measurement followed by an unconditional reset of the auxiliary, one would have access to error syndromes that can be used in a second layer of quantum error correction, without requiring fast feedback and feed-forward operations within the first layer.

In conclusion, we have demonstrated the preparation of GKP logical states in the mode of a superconducting cavity with state fidelities mainly limited by bit flips of the auxiliary and intrinsic dephasing of the storage mode. A quantum error correcting protocol based on reservoir engineering, in which the reset of the auxiliary serves as the dissipative process, is demonstrated. We have made the QEC protocol completely autonomous through the implementation of an unconditional auxiliary reset based on a dissipative swap to a lossy resonator. Despite the auxiliary having a relaxation time 10 times shorter than the storage mode, we demonstrate autonomous QEC of GKP states with a gain on the logical lifetime of about 24%. To guide the requirements at the second layer of error correction, further work is needed to upper bound the gain from QEC of the GKP code accessible with realistic hardware and software improvements.

---

[*]dany@nordquantique.ca

[1] S. Krinner, N. Lacroix, A. Remm, A. D. Paolo, E. Genois, C. Leroux, C. Hellings, S. Lazar, F. Swiadek, J. Herrmann, G. J. Norris, C. K. Andersen, M. Müller, A. Blais, C. Eichler, and A. Wallraff, Nature (London) **605**, 669 (2022).

[2] Y. Zhao *et al.*, Phys. Rev. Lett. **129**, 030501 (2022).

[3] N. Sundaresan, T. J. Yoder, Y. Kim, M. Li, E. H. Chen, G. Harper, T. Thorbeck, A. W. Cross, A. D. Córcoles, and M. Takita, Nat. Commun. **14**, 2852 (2023).

[4] G. Q. AI, Nature (London) **614**, 676 (2023).

[5] D. Gottesman, A. Kitaev, and J. Preskill, Phys. Rev. A **64**, 012310 (2001).

[6] V. V. Albert, K. Noh, K. Duivenvoorden, D. J. Young, R. T. Brierley, P. Reinhold, C. Vuillot, L. Li, C. Shen, S. M. Girvin, B. M. Terhal, and L. Jiang, Phys. Rev. A **97**, 032346 (2018).

[7] K. Noh and C. Chamberland, Phys. Rev. A **101**, 012316 (2020).

[8] W. L. Ma, S. Puri, R. J. Schoelkopf, M. H. Devoret, S. M. Girvin, and L. Jiang, Sci. Bull. **66**, 1789 (2021).

[9] W. Cai, Y. Ma, W. Wang, C. L. Zou, and L. Sun, Fundam. Res. **1**, 50 (2021).

[10] A. L. Grimsmo and S. Puri, PRX Quantum **2**, 020101 (2021).

[11] A. J. Brady, A. Eickbusch, S. Singh, J. Wu, and Q. Zhuang, Prog. Quantum Electron. **93**, 100496 (2024).

[12] N. Ofek, A. Petrenko, R. Heeres, P. Reinhold, Z. Leghtas, B. Vlastakis, Y. Liu, L. Frunzio, S. M. Girvin, L. Jiang, M. Mirrahimi, M. H. Devoret, and R. J. Schoelkopf, Nature (London) **536**, 441 (2016).

[13] L. Hu, Y. Ma, W. Cai, X. Mu, Y. Xu, W. Wang, Y. Wu, H. Wang, Y. P. Song, C. L. Zou, S. M. Girvin, L. M. Duan, and L. Sun, Nat. Phys. **15**, 503 (2019).

[14] P. Campagne-Ibarcq, A. Eickbusch, S. Touzard, E. Zalys-Geller, N. E. Frattini, V. V. Sivak, P. Reinhold, S. Puri, S. Shankar, R. J. Schoelkopf, L. Frunzio, M. Mirrahimi, and M. H. Devoret, Nature (London) **584**, 368 (2020).

[15] J. M. Gertler, B. Baker, J. Li, S. Shirol, J. Koch, and C. Wang, Nature (London) **590**, 243 (2021).

[16] B. de Neeve, T. long Nguyen, T. Behrle, and J. P. Home, Nat. Phys. **18**, 296 (2022).

[17] V. V. Sivak, A. Eickbusch, B. Royer, S. Singh, I. Tsioutsios, S. Ganjam, A. Miano, B. L. Brock, A. Z. Ding, L. Frunzio, S. M. Girvin, R. J. Schoelkopf, and M. H. Devoret, Nature (London) **616**, 55 (2023).

[18] Z. Ni, S. Li, X. Deng, Y. Cai, L. Zhang, W. Wang, Z.-B. Yang, H. Yu, F. Yan, S. Liu, C.-L. Zou, L. Sun, S.-B. Zheng, Y. Xu, and D. Yu, Nature (London) **616**, 56 (2023).

[19] J. P. Barnes and W. S. Warren, Phys. Rev. Lett. **85**, 856 (2000).

[20] J. M. Lihm, K. Noh, and U. R. Fischer, Phys. Rev. A **98**, 012317 (2018).

[21] Y. Zeng, Z.-Y. Zhou, E. Rinaldi, C. Gneiting, and F. Nori, Phys. Rev. Lett. **131**, 050601 (2023).

[22] B. Royer, S. Singh, and S. M. Girvin, Phys. Rev. Lett. **125**, 260509 (2020).

[23] A. Blais, A. L. Grimsmo, S. M. Girvin, and A. Wallraff, Rev. Mod. Phys. **93**, 025005 (2021).

[24] M. Reagor, W. Pfaff, C. Axline, R. W. Heeres, N. Ofek, K. Sliwa, E. Holland, C. Wang, J. Blumoff, K. Chou, M. J. Hatridge, L. Frunzio, M. H. Devoret, L. Jiang, and R. J. Schoelkopf, Phys. Rev. B **94**, 014506 (2016).

[25] C. Axline, M. Reagor, R. Heeres, P. Reinhold, C. Wang, K. Shain, W. Pfaff, Y. Chu, L. Frunzio, and R. J. Schoelkopf, Appl. Phys. Lett. **109**, 042601 (2016).

[26] J. Koch, T. M. Yu, J. Gambetta, A. A. Houck, D. I. Schuster, J. Majer, A. Blais, M. H. Devoret, S. M. Girvin, and R. J. Schoelkopf, Phys. Rev. A **76,** 042319 (2007).

[27] P. Magnard, P. Kurpiers, B. Royer, T. Walter, J. C. Besse, S. Gasparinetti, M. Pechal, J. Heinsoo, S. Storz, A. Blais, and A. Wallraff, Phys. Rev. Lett. **121,** 060502 (2018).

[28] D. J. Egger, M. Werninghaus, M. Ganzhorn, G. Salis, A. Fuhrer, P. Müller, and S. Filipp, Phys. Rev. Appl. **10,** 044030 (2018).

[29] Y. Sunada, S. Kono, J. Ilves, S. Tamate, T. Sugiyama, Y. Tabuchi, and Y. Nakamura, Phys. Rev. Appl. **17,** 044016 (2022).

[30] A. Eickbusch, V. Sivak, A. Z. Ding, S. S. Elder, S. R. Jha, J. Venkatraman, B. Royer, S. M. Girvin, R. J. Schoelkopf, and M. H. Devoret, Nat. Phys. **18,** 1464 (2022).

[31] See Supplemental Material at http://link.aps.org/supplemental/10.1103/PhysRevLett.132.150607 for more details on the hardware architecture, numerical simulations, and analysis methods, which includes Refs. [32–38].

[32] M. Reagor, Ph. D. thesis, Yale University, 2015.

[33] C. H. Wang, K. Noh, J. Lebreuilly, S. M. Girvin, and L. Jiang, Phys. Rev. Appl. **15,** 044026 (2021).

[34] F. Motzoi, J. M. Gambetta, P. Rebentrost, and F. K. Wilhelm, Phys. Rev. Lett. **103,** 110501 (2009).

[35] D. C. McKay, C. J. Wood, S. Sheldon, J. M. Chow, and J. M. Gambetta, Phys. Rev. A **96,** 022330 (2017).

[36] F. Mallet, F. R. Ong, A. Palacios-Laloy, F. Nguyen, P. Bertet, D. Vion, and D. Esteve, Nat. Phys. **5,** 791 (2009).

[37] K. Geerlings, Z. Leghtas, I. M. Pop, S. Shankar, L. Frunzio, R. J. Schoelkopf, M. Mirrahimi, and M. H. Devoret, Phys. Rev. Lett. **110,** 120501 (2013).

[38] S. Haroche and J.-M. Raimond, *Exploring the Quantum* (Oxford University Press, New York, 2006).

[39] C. Flühmann and J. P. Home, Phys. Rev. Lett. **125,** 043602 (2020).

[40] I. Strandberg, Phys. Rev. Appl. **18,** 044041 (2022).

[41] M. A. Nielsen, Phys. Lett. A **303,** 249 (2002).

[42] B. M. Terhal, J. Conrad, and C. Vuillot, Quantum Sci. Technol. **5,** 043001 (2020).

[43] S. Zeytinoglu, M. Pechal, S. Berger, A. A. Abdumalikov, A. Wallraff, and S. Filipp, Phys. Rev. A **91,** 043846 (2015).

[44] A. P. Place *et al.*, Nat. Commun. **12,** 1779 (2021).

[45] S. Puri, A. Grimm, P. Campagne-Ibarcq, A. Eickbusch, K. Noh, G. Roberts, L. Jiang, M. Mirrahimi, M. H. Devoret, and S. M. Girvin, Phys. Rev. X **9,** 041009 (2019).

[46] M. Mirrahimi, Z. Leghtas, V. V. Albert, S. Touzard, R. J. Schoelkopf, L. Jiang, and M. H. Devoret, New J. Phys. **16,** 045014 (2014).

[47] R. Lescanne, M. Villiers, T. Peronnin, A. Sarlette, M. Delbecq, B. Huard, T. Kontos, M. Mirrahimi, and Z. Leghtas, Nat. Phys. **16,** 509 (2020).

[48] A. Grimm, N. E. Frattini, S. Puri, S. O. Mundhada, S. Touzard, M. Mirrahimi, S. M. Girvin, S. Shankar, and M. H. Devoret, Nature (London) **584,** 205 (2020).

[49] N. E. Frattini, R. G. Cortiñas, J. Venkatraman, X. Xiao, Q. Su, C. U. Lei, B. J. Chapman, V. R. Joshi, S. M. Girvin, R. J. Schoelkopf, S. Puri, and M. H. Devoret, arXiv:2209.03934.

[50] U. Réglade, A. Bocquet, R. Gautier, A. Marquet, E. Albertinale, N. Pankratova, M. Hallén, F. Rautschke, L.-A. Sellem, P. Rouchon, A. Sarlette, M. Mirrahimi, P. Campagne-Ibarcq, R. Lescanne, S. Jezouin, and Z. Leghtas, arXiv:2307.06617.

[51] B. Royer, S. Singh, and S. M. Girvin, PRX Quantum **3,** 010335 (2022).

[52] N. Didier, J. Bourassa, and A. Blais, Phys. Rev. Lett. **115,** 203601 (2015).

[53] A. Eddins, S. Schreppler, D. M. Toyli, L. S. Martin, S. Hacohen-Gourgy, L. C. G. Govia, H. Ribeiro, A. A. Clerk, and I. Siddiqi, Phys. Rev. Lett. **120,** 040505 (2018).

[54] S. Touzard, A. Kou, N. E. Frattini, V. V. Sivak, S. Puri, A. Grimm, L. Frunzio, S. Shankar, and M. H. Devoret, Phys. Rev. Lett. **122,** 080502 (2019).

[55] J. Ikonen, J. Goetz, J. Ilves, A. Keränen, A. M. Gunyho, M. Partanen, K. Y. Tan, D. Hazra, L. Grönberg, V. Vesterinen, S. Simbierowicz, J. Hassel, and M. Möttönen, Phys. Rev. Lett. **122,** 080503 (2019).

[56] A. A. Diringer, E. Blumenthal, A. Grinberg, L. Jiang, and S. Hacohen-Gourgy, arXiv:2301.09831.